Inorganic Chemistry

pubs.acs.org/IC

Article

Asymmetrically Coordinated Heterodimetallic Ir−Ru System: Synthesis, Computational, and Anticancer Aspects

Saumyaranjan Mishra, Suman Kumar Tripathy, Debasish Paul, Paltan Laha, Manas Kumar Santra,* and Srikanta Patra*

Cite This: *Inorg. Chem.* 2023, 62, 7003−7013

Read Online

ACCESS | Metrics & More | Article Recommendations | Supporting Information

ABSTRACT: Herein, we present an unprecedented formation of a heterodinuclear complex $[\{(ppy)_2Ir^{III}\}(\mu\text{-phpy})\{Ru^{II}(tpy)\}](ClO_4)_2$ $\{[\mathbf{1}](ClO_4)_2\}$ using terpyridyl/phenylpyridine as ancillary ligands and asymmetric phpy as a bridging ligand. The asymmetric binding mode (N^N-∩-N^N^C$^-$) of the phpy ligand in $\{[\mathbf{1}](ClO_4)_2\}$ is confirmed by ^{1}H, ^{13}C, ^{1}H−^{1}H correlated spectroscopy (COSY), high-resolution mass spectrum (HRMS), single-crystal X-ray crystallography techniques, and solution conductivity measurements. Theoretical investigation suggests that the highest occupied molecular orbital (HOMO) and the least unoccupied molecular orbital (LUMO) of $[\mathbf{1}]^{2+}$ are located on iridium/ppy and phpy, respectively. The complex displays a broad low energy charge transfer (CT) band within 450−575 nm. The time-dependent density functional theory (TDDFT) analysis suggests this as a mixture of metal-to-ligand charge transfer (MLCT) and ligand-to-ligand charge transfer (LLCT), where both ruthenium, iridium, and ligands are involved. Complex $\{[\mathbf{1}](ClO_4)_2\}$ exhibits $Ru^{II}Ir^{III}/Ru^{III}Ir^{III}$- and $Ru^{III}Ir^{III}/Ru^{III}Ir^{IV}$-based oxidative couples at 0.83 and 1.39 V, respectively. The complex shows anticancer activity and selectivity toward human breast cancer cells (IC_{50}; MCF-7: 9.3 ± 1.2 μM, and MDA-MB-231: 8.6 ± 1.2 μM) over normal breast cells (MCF 10A: $IC_{50} \approx 21 \pm 1.3$ μM). The Western blot analysis and fluorescence microscopy images suggest that combined apoptosis and autophagy are responsible for cancer cell death.

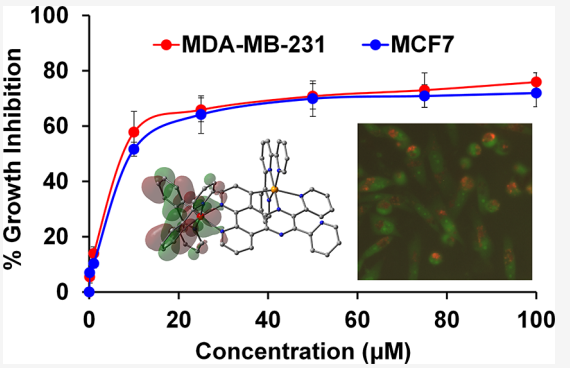

INTRODUCTION

The development of transition metal-based multimetallic systems with suitable ligand frameworks is a fascinating area of contemporary research. Such systems often display new/improved properties against their monometallic analogues and find diverse applications in chemistry and biology.[1−16] Recently, the exploration of such systems as anticancer agents[17−21] has gained serious momentum with the success of their mononuclear analogues. In addition, they have demonstrated a significant improvement in anticancer activity and exhibit a different mechanism of cell death compared to cisplatin.[17,18]

Alternatively, an entailed approach of combining different cytotoxic units into a single molecular framework is exciting, as they combine the properties of individual therapeutic units, which may exhibit improved pharmacological profiles.[22,23] In addition, such scaffolds offer synchronous delivery to the target site eliminating multiple drug combinations. Although a plethora of homometallic di- and multinuclear systems have been developed and studied, the exploration of heterometallic systems is relatively less. A few examples of the combination of metals such as Ru−Ti,[22] Ru−Co,[24−26] Ru−Ni,[26] Ru−Zn,[26] Ru−Fe,[27] Ru−Au,[28−32] Ru−Sn,[33] Ru−Pt,[34−37] Ru−Sm,[38] Ti−Au,[25,39,40] Ti−Pd,[41] Fe−Pd,[42,43] Fe−Au,[42,44] Cu−Au,[45] Co−Au,[46] Re−Au,[47,48] Re−Pt,[49] Au−Ir,[50] Os−Ir,[51] Eu−Pt,[52] Ti−Au−Ti,[40] Au−Ti−Au,[39,41] Ti−Au−Fe,[53] Pt−Ru−Pt,[34] Au−Ru−Au,[54] etc. have been developed, and their anticancer activity is studied extensively. In addition to exhibiting better anticancer activity, multimetallic systems are also found to target different intracellular organs other than nucleic acid, leading to an alternative mode of action.[22,28−30,37,42,44,55]

Interestingly, a combination of Ru and Ir has rarely been explored in this aspect, although their mononuclear analogues are well known for their interesting photophysical and photochemical properties, stability, efficient DNA intercalating ability, biological activity, etc.[23,56]

Nevertheless, polynucleating pyrazine-based ligands have been extensively used for the development of multimetallic assemblies. Most of the ligand frameworks used are either rigid or flexible. Ligands having rigid and flexible frameworks with variable coordination sites are relatively uncommon.[57−62] The

Received: January 25, 2023
Published: April 25, 2023

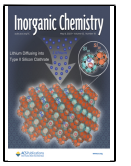

https://doi.org/10.1021/acs.inorgchem.3c00272
Inorg. Chem. 2023, 62, 7003−7013

polypyridyl-pyrazine-based 2,3-di(pyridin-2-yl)pyrazino[2,3-*f*][1,10] phenanthroline (phpy) ligand offers a rigid framework at the phenanthroline end and flexible donors sites at the pyrazine end. The flexible pyridine donors at the pyrazine end can potentially coordinate with the same/different metals in various coordination modes (Chart 1).

Chart 1. Different Metal Binding Modes of the phpy Ligand

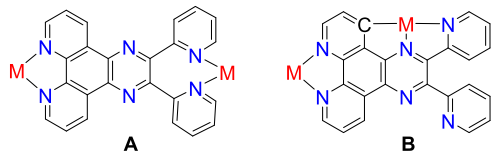

In general, Ru center coordinates with polypyridyl ligands through neutral N^N donor sites (Chart 1A).[23] Binding of Ru through anionic N^N^C$^-$/N^C$^-$ donor sites of polypyridyl ligands are less common (Chart 1B).[63−65] Bridging ligands functioning as asymmetric N^N and N^N^C$^-$/N^C$^-$ donors are rare.[66−70] Further, the study of heterodinuclear Ru−Ir complex bridged through asymmetric N^N and N^N^C$^-$ bridging ligands is not known. Thus, the present study intends to highlight the formation of a heterodinuclear (Ir−Ru) complex, where Ru center forms the cyclometalated complex (Ru−C) with the phpy ligand and their cytotoxic activity against various cancer cells.

Herein, we report the synthesis of a cyclometalated heterodinuclear complex [{(ppy)$_2$Ir^{III}}(μ-phpy){Ru^{II}(tpy)}](ClO$_4$)$_2$ {[**1**](ClO$_4$)$_2$} incorporating pyridyl-based ligands (tpy = 2,2′:6′,2″-terpyridine; ppy= 2-phenylpyridine; phpy = 2,3-di(pyridin-2-yl)pyrazino[2,3-*f*][1,10] phenanthroline). The characterization and physicochemical properties of complex {[**1**](ClO$_4$)$_2$} are carried out using various analytical techniques. The density functional theory (DFT) study of [**1**]$^{2+}$ has been conducted to determine the geometric structure and vertical excitation energies to verify the origin of the experimentally observed bands in the UV−vis spectrum. The anticancer activity of complex {[**1**](ClO$_4$)$_2$} is studied using MCF-7 (p53 wild) and MDA-MB-231 (p53 mutant) cell lines. Moreover, the mechanism of cancer cell death has been established via fluorescence-activated cell sorting (FACS), Western blot analysis, and confocal microscopy techniques.

RESULTS AND DISCUSSION

The dinucleating ligand 2,3-di(pyridin-2-yl)pyrazino[2,3-*f*][1,10] phenanthroline (phpy) is prepared by the condensation reaction between 5,6-diamino-1,10-phenanthroline with commercially available 2,2′-bipyridyl.[23,62] The heterodinuclear {[**1**](ClO$_4$)$_2$} is synthesized first by reacting the phpy ligand with dimeric precursor [(ppy)$_2$Ir^{III}(μ-Cl)]$_2$ (1:0.5 mole ratio),[62] followed by its purification and further reaction with [Ru^{III}(tpy)Cl$_3$] (1:1 mole ratio) (see Experimental Section) (Scheme 1). Complex {[**1**](ClO$_4$)$_2$} is isolated as its ClO$_4$ salt. The complex is soluble in most of the polar organic solvents and is sufficiently stable in the air.

The diamagnetic {[**1**](ClO$_4$)$_2$} is 1:2 electrolyte in the CH$_3$CN solution. The presence of ClO$_4^-$ counteranion is evidenced by observing the characteristic ν(ClO$_4^-$) infrared vibrations at 1100 and 670 cm^{-1}. Apparently, from the conductivity data, it appears that complex {[**1**](ClO$_4$)$_2$} is formed with binding mode **A** as shown in Chart 1. Accordingly, complex {[**1**](ClO$_4$)$_2$} should exhibit a molecular ion peak centered at 1356.1393 (corresponding {[**1**]ClO$_4$}$^+$). Surprisingly, the high-resolution mass spectrum of {[**1**]ClO$_4$}$^+$ shows a molecular ion peak centered at 1320.1653 (calculated 1320.1628), which is ∼36 units less than the expected molecular mass (Figure 1). This suggests the alternative

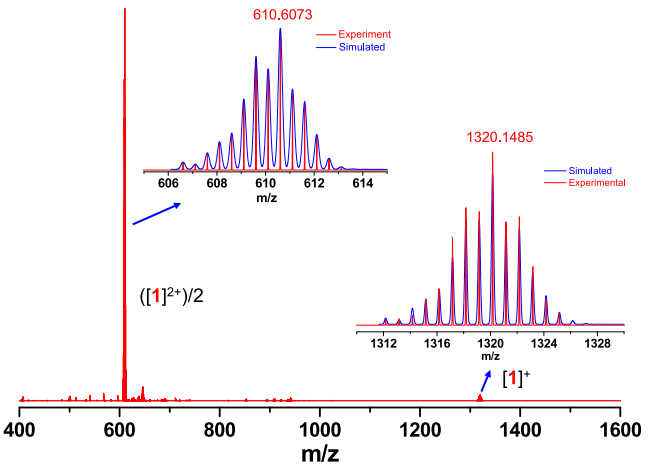

Figure 1. High-resolution mass spectrum (HRMS) of {[**1**]ClO$_4$}$^+$ in CH$_3$CN. The inset represents the expanded molecular ion peak (red) and its simulated pattern (blue).

formulation **B**, as shown in Chart 1, where complex {[**1**](ClO$_4$)$_2$} loses one Cl$^-$ ligand and an H atom from the bridging ligand (phpy). The phpy ligand gets deprotonated and coordinates with [(tpy)Ru] unit through an unusual

Scheme 1. Scheme for the Synthesis of Heterodimetallic Complex 1

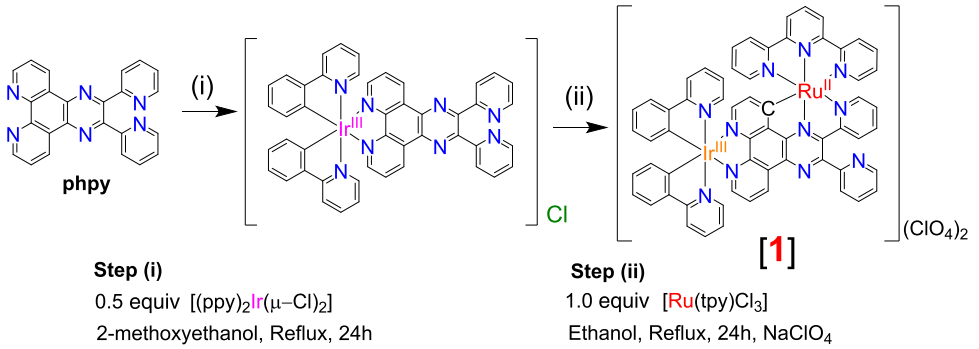

https://doi.org/10.1021/acs.inorgchem.3c00272
Inorg. Chem. 2023, 62, 7003−7013

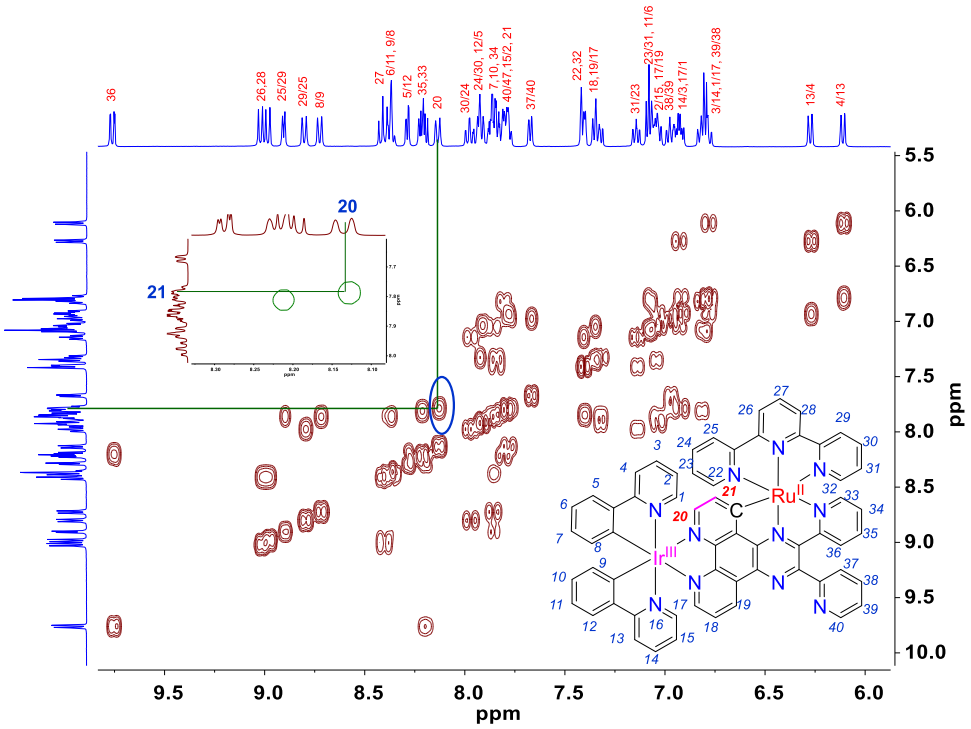

Figure 2. $^{1}H-^{1}H$ correlated spectroscopy (COSY) spectrum of complex $[\mathbf{1}](ClO_4)_2$ in DMSO-d_6.

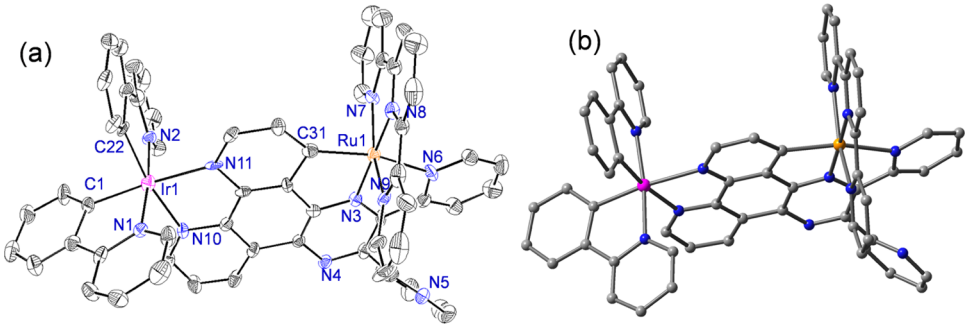

Figure 3. (a) ORTEP and (b) geometry-optimized structure (in the gas phase) of complex $[\mathbf{1}]^{2+}$. Ellipsoids are drawn at a 20% probability level. Hydrogen atoms and counteranions are eliminated for clarity.

N^N^C$^-$ binding mode (Chart 1B). This type of asymmetric N^N and N^N^C$^-$ coordination mode of the phpy ligand is not observed before. The molecular ion peak of $\{[\mathbf{1}](ClO_4)\}^+$ nicely matches with the simulated mass pattern, which further supports the formation of the complex with unusual binding mode of [(tpy)Ru] with the distal unit of the phpy ligand (Chart 1B). Hence, the molecular structure of complex $\{[\mathbf{1}](ClO_4)_2\}$ could be formulated as $[\{(ppy)_2Ir^{III}\}(\mu\text{-phpy})\{Ru^{II}(tpy)\}](ClO_4)_2$ (Chart 1).

The solution identity of complex $\{[\mathbf{1}](ClO_4)_2\}$ is confirmed by ^{1}H and ^{13}C NMR spectroscopy (Figure S1). The complex has shown the desired number of protons (40) within 0−10 ppm in its ^{1}H NMR spectrum, indicating the presence of phpy, ppy, and tpy ligands and confirming its unusual binding mode (Chart 1B). The ^{13}C NMR spectrum of $[\mathbf{1}](ClO_4)_2$ displays three distinct signals at 202.6, 167.1, and 166.9 ppm, which correspond to the binding carbon centers of phpy with ruthenium and ppy with iridium, respectively. A similar type of observation for cyclometalated complexes has also been reported previously.[55,57,62,64,71] This further affirms the Ru−C coordination in complex $[\mathbf{1}](ClO_4)_2$. The $^{1}H-^{1}H$ correlation spectroscopy study was conducted (Figure 2) to elucidate further the structural aspect of complex $[\mathbf{1}](ClO_4)_2$. Because of the presence of several aromatic protons of a similar chemical environment, the peaks are not well resolved, and some of them are overlapped. Fortunately, complex $[\mathbf{1}](ClO_4)_2$ possesses two distinct protons (20 and 21), which only correlate with each other due to the absence of neighboring protons and should appear as a doublet. Two doublets at 8.13 ppm and 7.79 ppm are detected and correlate with each other. This further supports the Ru−C coordination in complex $[\mathbf{1}](ClO_4)_2$.

The single-crystal X-ray crystallographic analysis was conducted to get more insight into the structure and unusual bond formation. The X-ray quality crystals were grown in dimethyl sulfoxide (DMSO) at room temperature. The oak ridge thermal ellipsoid plot (ORTEP) diagram of complex $[\mathbf{1}](ClO_4)_2$ is shown in Figure 3a, and important crystallographic parameters are listed in Tables TS1 and TS2. Complex $[\mathbf{1}](ClO_4)_2$ was crystallized out in a triclinic crystal system with the $P\bar{1}$ space group. From the crystal structure, it is observed that $[(ppy)_2Ir]$ is coordinated to the rigid part,

https://doi.org/10.1021/acs.inorgchem.3c00272
Inorg. Chem. 2023, 62, 7003−7013

whereas the [Ru(tpy)] unit is coordinated to the flexible part of the phpy ligand (Figure 3a). It is interesting to note that the phpy ligand offers a tridentate N^N^C$^-$ coordination mode while coordinating with [Ru(tpy)]. However, it showed a neutral N^N-∩-N^N binding mode when the [(*p*-cym)RuCl] fragment is used.[23] Change in the coordination mode by varying the *p*-cym ligand to the tpy ligand is a quite remarkable observation. This type of unusual anionic ditopic N^N and N^N^C$^-$ coordination mode displayed by the phpy ligand is not seen before. The Ir^1−N^{10}/N^{11} distances (2.148−2.133 Å) are found to be longer than the Ir^1−N^1/N^2 distances (1.992−2.047 Å), which is due to the *trans*-directing effect of the anionic C center of the ppy ligands. The N−Ir1−N and N−Ir1−C bond angles are in line with the structurally similar iridium complexes.[23,55−57,62,64] On the other hand, the Ru^1−N^7/N^8/N^9(tpy) (1.937−2.092 Å) distances are quite shorter than Ru^1−N^6 (2.65 Å), which is again the *trans*-directing effect of the phenanthroline C(C31) unit of the phpy ligand. This further confirms the Ru−C coordination of the [Ru(tpy)] unit with the phpy ligand.

The equilibrium geometry of [**1**]$^{2+}$ has been calculated at the level of density functional theory (DFT) using the B3LYP hybrid functional. The optimized geometry and related bond parameters of complex [**1**]$^{2+}$ are displayed in Figure 3b and Tables TS3−TS5. From the DFT analysis, it is observed that the pyridine rings of the phpy ligand deviate from planarity. However, the other ligands such as tpy and ppy are planner, which is evident from the dihedral angles. The calculated Ru−N (1.99−2.15 Å), Ru−C (2.06 Å), Ir−N (2.06 Å), and Ir−C (2.02 Å) bond distances are in agreement with the experimentally observed (Table TS2) and structurally characterized similar complexes.[23,55,62,72−74] A slight deviation from the idealized geometries of both ruthenium and iridium centers in [**1**]$^{2+}$ is observed from the optimized geometrical parameters (Tables TS3−TS5).

Further, the nature and composition of frontier orbitals are analyzed from the optimized geometry. It is found that the highest occupied molecular orbital (HOMO) of the complex resides at −8.87 eV and is localized on the ppy (63%) unit and iridium center (35%) (Figure 4 and Table TS6). On the other hand, the least unoccupied molecular orbital is situated at −6.89 eV and localized mainly on the phpy ligand (90%). The HOMO−LUMO energy gap is 1.98 eV, which falls in the visible region (*vide infra*).

Experimentally, the heterodinuclear [**1**](ClO$_4$)$_2$ displays ligand-based transitions below 350 nm along with broad low-energy MLCT bands in the visible region (400−600 nm) (Figure 5a).[75−80] It is difficult to exactly assign the MLCT transitions from the ruthenium or iridium center. Cyclometalated {Ir(ppy)$_2$} centers generally show an MLCT band around or below 400 nm.[23,62,76−78,80] Thus, the low-energy bands for [**1**](ClO$_4$)$_2$ could be assigned to the RuN$_5$C → phpy/tpy MLCT transition.[65] To get more insight into the electronic transitions, TDDFT analysis using the optimized geometry was conducted. This reveals that the broad low-energy band is composed of a mixture of MLCT and LLCT transitions [Ru$_{(d\pi)}$/ppy$_{(\pi)}$/tpy$_{(\pi)}$ → phpy$_{(\pi^*)}$; Ir$_{(d\pi)}$/ppy$_{(\pi)}$ → phpy$_{(\pi^*)}$; ppy$_{(\pi)}$ → phpy$_{(\pi^*)}$/tpy$_{(\pi)^*}$], where ruthenium, iridium, and ligands are involved (Table TS7).

Complex [**1**](ClO$_4$)$_2$ displays two quasi-reversible redox couples, $E_{1/2}$, at 0.83 and 1.39 V, which may be attributed to Ru^{II}Ir^{III}/Ru^{III}Ir^{III} (RuN$_5$C center) and Ru^{III}Ir^{III}/Ru^{III}Ir^{IV} (IrN$_4$C$_2$ center) oxidation, respectively (Figure 5b). Complex

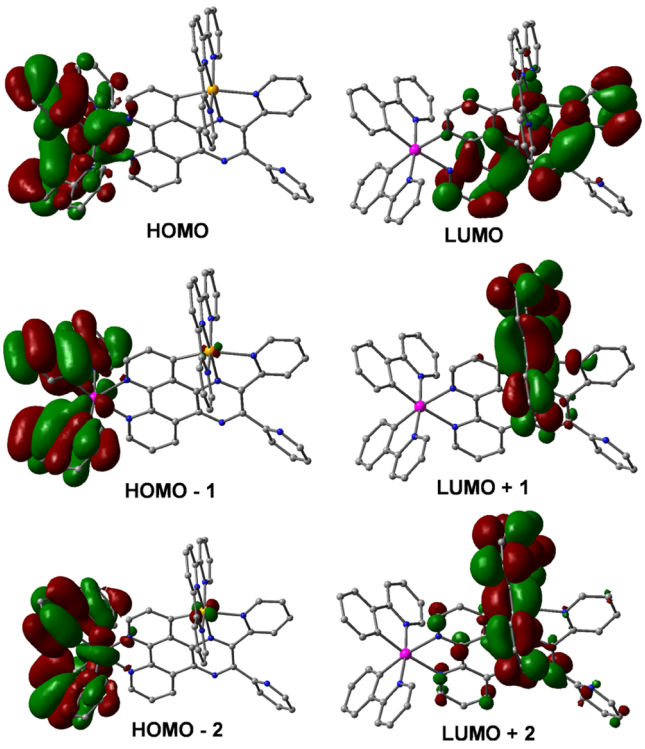

Figure 4. Pictorial representation of the Kohn−Sham orbitals of [**1**]$^{2+}$ in the gas phase.

[**1**](ClO$_4$)$_2$ also shows the reduction of the phenanthroline unit of the phpy ligand at the negative potential of the cyclic voltammogram.

Both ruthenium and iridium complexes are known to exhibit excellent anticancer activity toward various cancer cells.[17,22,81−84] Thus, the anticancer activity of [**1**](ClO$_4$)$_2$ is tested using two breast cancer cell lines: non-metastatic MCF-7 and highly metastatic triple-negative breast cancer cell line MDA-MB-231 by using standard 3-(4,5-dimethylthiazol-2-yl)-2,5-diphenyltetrazolium bromide (MTT) assay (Figures 6a and S3). The IC$_{50}$ values of [**1**](ClO$_4$)$_2$ against cancer cells are gathered in Table 1.

Complex [**1**](ClO$_4$)$_2$ shows a significantly higher antiproliferative activity against both cancer cell lines as compared to the standard cisplatin. Moreover, data reveals that complex [**1**](ClO$_4$)$_2$ is more active against MCF-7 cells compared to MDA-MB-231 cells. Interestingly, complex [**1**](ClO$_4$)$_2$ displays moderately less toxicity toward normal breast cells (MCF 10A) (IC$_{50}$ ≈ 21 ± 1.3 μM), suggesting its selectivity toward cancer cells (Table 1).

Next, we studied the stability of the complex in a phosphate buffer saline solution. It is found that all of the complexes are reasonably stable in buffer solution at least for 48 h (Figure S2).

To understand the molecular mechanism of the anticancer activity of complex [**1**](ClO$_4$)$_2$, fluorescence-activated cell sorting (FACS) analysis was conducted (Figure S4). A significant amount (73%) of the cell population is observed at the sub-G1 phase after 48 h of treatment of [**1**](ClO$_4$)$_2$, indicating the apoptotic mode of cell death. Further, the Western blot analysis for the marker proteins, such as Apaf1, cleaved caspase 3, PUMA, etc., responsible for apoptosis, are examined (Figure 6b,c). It is observed that the expression levels of Apaf1, cleaved caspase 3 in MCF-7 cells, and Apaf1,

https://doi.org/10.1021/acs.inorgchem.3c00272
Inorg. Chem. 2023, 62, 7003−7013

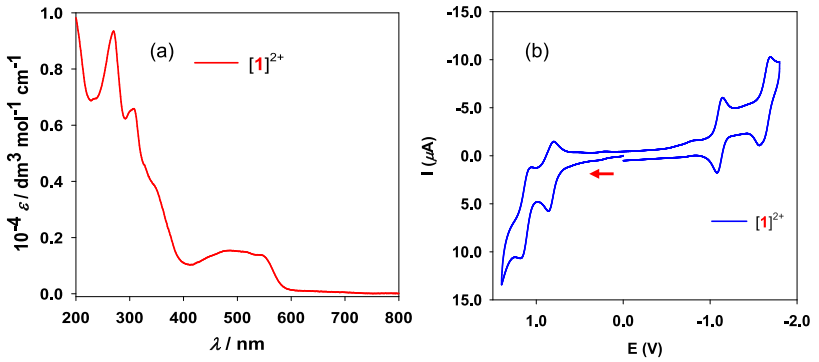

Figure 5. (a) UV−vis and (b) cyclic voltammogram of complex $[\mathbf{1}](ClO_4)_2$ in CH_3CN.

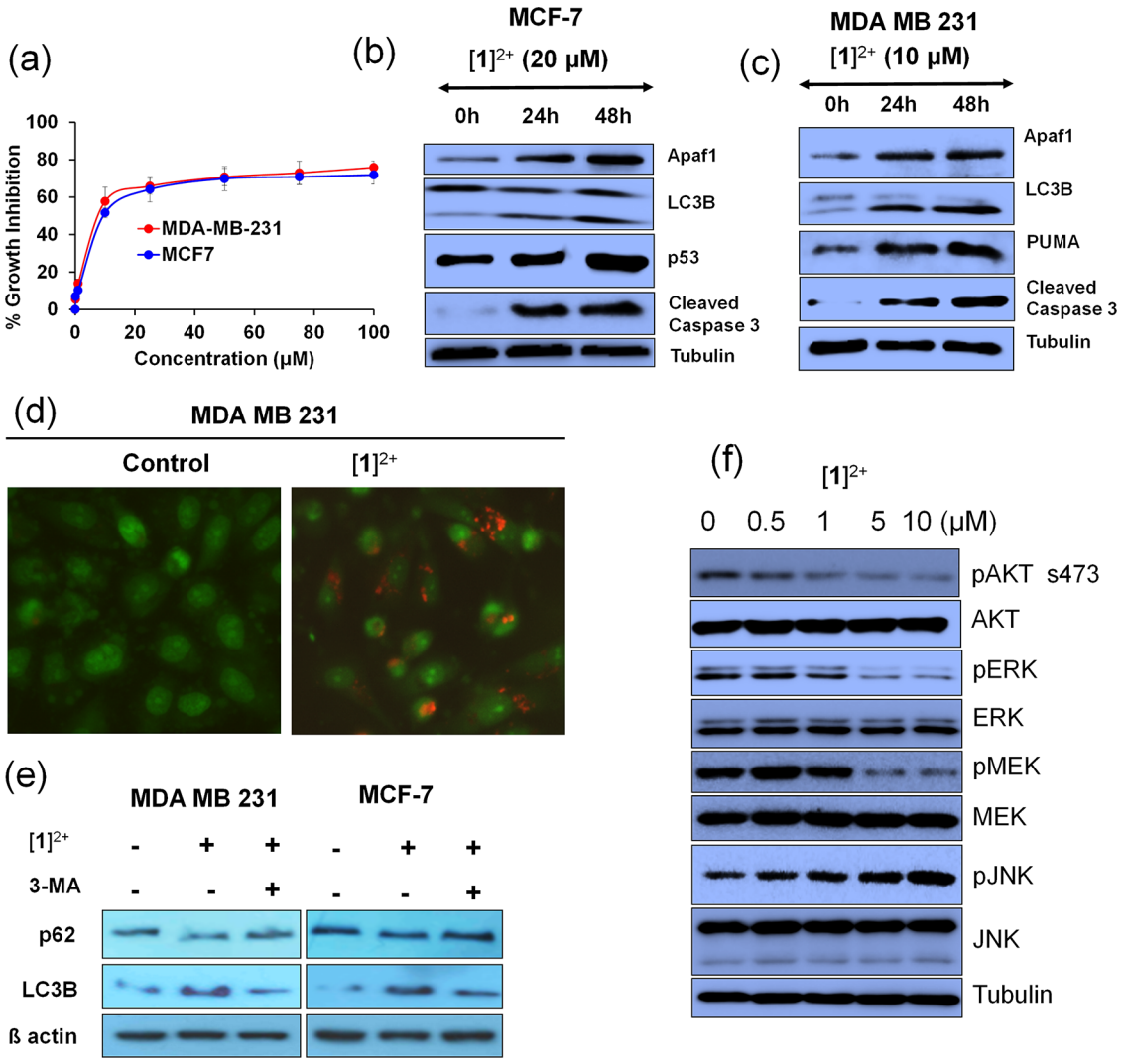

Figure 6. (a) Dose-dependent suppression of cell viability of complex $[\mathbf{1}](ClO_4)_2$ in human breast MCF-7 and MDA-MB-231 cancer cell lines. The graph represents the average of three biological replicates. (b, c) Expression levels of marker proteins involved in apoptosis and autophagy were analyzed by immunoblotting assay. (d) Fluorescence microscopic images of MDA-MB-231 cancer cells treated with acridine orange in the absence (left) and presence (right) of $[\mathbf{1}](ClO_4)_2$ (5 μM). (e) Expression levels of autophagic marker proteins were examined by immunoblotting in the absence and presence of autophagic inhibitor 3-methyladenine (3-MA). (f) Expression levels of kinases were examined following the treatment of complex $[\mathbf{1}](ClO_4)_2$ at the indicated concentration.

cleaved caspase 3, and PUMA in MDA-MB-231 cells are increased (Figure 6b,c), indicating that cells undergo apoptotic cell death following the treatment with $[\mathbf{1}](ClO_4)_2$.

In addition to apoptotic cell death, previous studies showed that organometallic compounds also induce autophagic cell death.[18,21] We, therefore, examined whether complex $[\mathbf{1}](ClO_4)_2$ has a role in autophagic cell death. A significant

https://doi.org/10.1021/acs.inorgchem.3c00272
Inorg. Chem. 2023, 62, 7003−7013

Table 1. In Vitro Growth Inhibition against Human Breast Cancer (MCF-7 and MDA-MB-231) and Normal Breast (MCF 10A) Cell Lines and the Hydrophobicity of Complex $[1](ClO_4)_2$

complexes	MCF-7[a]	MDA-MB-231[a]	MCF 10A	$\frac{C_{n-octanol}}{C_{water}}$
$[1](ClO_4)_2$	9.3 ± 1.2	8.6 ± 1.2	21.2 ± 1.3	1.22
[Ir]	17.8 ± 4.8	ND	ND	ND
[Ru]	89.0 ± 9.8	ND	ND	ND
[Ir] + [Ru]	19.1 ± 3.1	ND	ND	ND
Phpy	>100	ND	ND	ND
Cisplatin	35.5 ± 7.2	ND	ND	ND

[a]IC_{50} values are in μM; ND: not determined. [Ir] ≈ $[(ppy)_2Ir(phpy)](ClO_4)$; [Ru] ≈ $[(tpy)Ru(phpy)Cl](ClO_4)$.

increase in LC3B II is observed in both cell lines, indicating that the autophagy mode of action is also functioning (Figure 6b,c). Moreover, the microscopic analysis of MDA-MB-231 cells treated with $[1](ClO_4)_2$ reveals the formation of acidic vacuoles (Figure 6d).

To further confirm the autophagy mode of cell death, the cells were treated with autophagy inhibitor 3-methyladenine (3-MA). It is observed that $[1](ClO_4)_2$ treatment increases the level of LC3B II, which is significantly reduced upon the 3-MA treatment, suggesting that $[1](ClO_4)_2$ induces autophagic cells also (Figure 6e). Thus, collectively the data suggests that complex $[1](ClO_4)_2$ induces both apoptosis and autophagy modes of cell death in both MCF-7 and MDA-MB-231 cancer cell lines.

It should be noted that both mononuclear cyclometalated iridium complex $[(ppy)_2Ir^{III}(phpy)]^+$ and heterodimetallic iridium−ruthenium complex $[(ppy)_2Ir^{III}(\mu\text{-phpy})(p\text{-cym})Ru^{II}Cl]^{2+}$ with the same phpy ligand display a similar anticancer activity (IC_{50} values 0.86 and 0.91 μM, respectively) and exhibit paraptotic and autophagic modes of cell death, respectively.[23,62] However, in the present study, replacing *p*-cymene with terpyridine (tpy) ligand and keeping other metals and ligands the same cause the mechanism of action to change from autophagy to a combination of apoptosis and autophagy. Thus, mere variation of ligand can modulate the mode of action.

Previous studies showed that AKT, MAPK, and JNK signaling pathways play a critical role in apoptotic as well as autophagic cell death.[85−89] We found that $[1](ClO_4)_2$ also induces apoptotic as well as autophagic cells. We then investigated whether $[1](ClO_4)_2$ induces cell death by altering the activity of these kinases. Immunoblotting results demonstrate that complex $[1](ClO_4)_2$ suppresses the activity of cell death inhibitory AKT and MAPK kinases (Figure 6f). In addition, we observe that complex $[1](ClO_4)_2$ has a more potent suppressive effect on AKT as compared to MAPK. For example, as compared to phosphorylated MEK-ERK, phosphorylation of AKT is significantly suppressed upon treatment of 1 μM of complex $[1](ClO_4)_2$ (Figure 6f). It is well known that the inhibition of AKT or activation of JNK leads to the induction of apoptosis.[89,90] Thus, our data revealed that complex $[1](ClO_4)_2$ induces cell death in part by inhibiting growth-promoting kinases.

CONCLUSIONS

In conclusion, cyclometalated heterodinuclear complex $[1](ClO_4)_2$ of Ru and Ir has been developed by using terpyridyl and 2-phenylpyridine as ancillary ligands and asymmetric phpy as the bridging ligand. The complex is characterized by various analytical techniques. The unusual Ru−C binding mode is confirmed by single-crystal X-ray crystallography, HRMS, ^{13}C NMR, and COSY techniques. The iridium center is coordinated through normal N^N binding mode at the phenanthroline end, whereas the ruthenium is coordinated through the unusual N^N^C$^-$ coordination mode at the pyrazine end. Theoretical investigation suggests that the HOMO is mainly localized on the Ir and ppy, whereas the LUMO resides on the phpy ligand. Complex $[1](ClO_4)_2$ displays better anticancer activity against human breast cancer cell lines MCF-7 and MDA-MB-231 as compared to cisplatin. The FACS and Western blot analyses reveal that the complex induces both apoptosis and autophagy. Complex $[1](ClO_4)_2$ has moderate selectivity toward human breast cancer cells than toward normal breast cells (IC_{50} = 9.3 ± 1.2 μM for MCF-7 and IC_{50} ∼ 21.2 ± 1.3 μM for MCF 10A).

Most of the cancer cells are cell death resistant due to the aberrant activation of kinases like AKT and MAP kinase. Of note, AKT is aberrantly activated in the majority of breast cancers.[89] Our finding reveals that $[1](ClO_4)_2$ inactivates cell death resistance kinases but activates cell-death-promoting kinase JNK to induce cell death. Metal complex inducing cancer cell death through the nonapoptotic mode is very important for the treatment of resistant cancer. Our earlier observation shows that the use of *p*-cymene $[(ppy)_2Ir^{III}(\mu\text{-phpy})(p\text{-cym})Ru^{II}Cl]^{2+}$ leads to autophagy,[23] whereas in the present work, the heterodimetallic complex with the terpyridine ligand displays combined apoptosis and autophagy. Moreover, the mononuclear iridium complex $[(ppy)_2Ir^{III}(phpy)]^+$ shows paraptosis.[62] Further, mere variation of ancillary ligand and selection of metal can modulate the mode of action to a great extent. Thus, the present contribution provides a unique example that would be useful for the development of anticancer agents for the treatment of resistant cancer.

EXPERIMENTAL SECTION

Materials. The precursor complexes $[Ru(tpy)Cl_3]$,[74,91] $[(ppy)_2Ir(\mu\text{-Cl})]_2$,[92] and 5,6-diamino-1,10-phenanthroline[93] were prepared by following the reported procedures. The bridging ligand 2,3-di(pyridin-2-yl)pyrazino[2,3-*f*][1,10] phenanthroline (phpy) ligand was synthesized by following the reported procedure.[23,60,62] The mononuclear $[(ppy)_2Ir(phpy)](ClO_4)$ was prepared by following the procedure reported earlier.[23,62] All chemicals were purchased from commercial sources and used as received. The solvents were dried by conventional methods and distilled prior to use. All culture media and supplements for cell work were purchased from Gibco Invitrogen Corporation (CA).

Instrumentation. The conductivity measurement was done using the OAKton PC2700 conductivity bridge. The UV−vis spectrum was obtained by using a Perkin Elmer Lambda 35 spectrophotometer. The FTIR spectrum was recorded using a Bruker α FTIR spectrophotometer with the sample prepared as the KBr pellet. Mass spectra were acquired on a Thermo Fisher Scientific Q Exactive Plus Orbitrap mass spectrometer. ^1H NMR spectrum was acquired on a Bruker Avance III 400 spectrometer using the DMSO-d_6 solvent. Electrochemical measurement was carried out in a dinitrogen atmosphere using a CHI 6205 electrochemical analyzer with Et_4NClO_4 as the supporting electrolyte (0.1 M), and the solute concentration was 10^{-3} M. For electrochemical measurements, a glassy carbon working electrode, Pt wire counter electrode, and Ag/AgCl as the reference electrode were used. The half-wave potential $E_{298\,K}$ was set equal to $0.5(E_{pa} + E_{pc})$, where E_{pa} and E_{pc} are anodic and cathodic cyclic

https://doi.org/10.1021/acs.inorgchem.3c00272
Inorg. Chem. 2023, 62, 7003−7013

voltammetric peak potentials, respectively. In this cell, F_c/F_c^+ couple had an $E_{1/2}$ value of 0.22 V.

Synthesis of [(ppy)$_2$Ir(μ-phpy)Ru(tpy)](ClO$_4$)$_2$ ([1](ClO$_4$)$_2$). The mononuclear iridium complex [(ppy)$_2$Ir(phpy)](ClO$_4$) (51.5 mg, 0.05 mmol) and [(tpy)Ru^{III}Cl$_3$] (22.0 mg, 0.05 mmol) precursor were taken in 1:1 ratio in dry ethanol, followed by 34 μL of NEt$_3$, and refluxed for 12 h under dinitrogen atmosphere. The volume of the solution was reduced under vacuum and a saturated solution of aqueous NaClO$_4$ was added to it, which gave a reddish-brown precipitate. It was further filtered, washed with enough cold distilled water, and dried in air. Pure [**1**](ClO$_4$)$_2$ was obtained by column chromatography using neutral alumina as a support and a mixture of solvent CH_2Cl_2: CH_3CN (2:1). Yield: 47 mg (66%). Molar conductivity [$\Lambda_M/(\Omega^{-1}$ cm^2 M^{-1})] in CH_3CN: 198. HRMS ((+)-ESI): m/z 1320.1653 corresponding to {[**1**]ClO$_4$}$^+$ (calculated molecular mass for 1320.1628). ^{1}H NMR (400 MHz,) δ/ppm: 9.72 (dd, J = 8.3, 1.4 Hz, 1H), 8.98 (d, J = 8.1 Hz, 1H), 8.94 (d, J = 4.2 Hz, 1H), 8.88−8.84 (m, 1H), 8.76 (d, J = 8.2 Hz, 1H), 8.69 (d, J = 8.2 Hz, 1H), 8.41−8.29 (m, 3H), 8.25 (dd, J = 5.2, 1.4 Hz, 1H), 8.20−8.13 (m, 2H), 8.10 (d, J = 8.3 Hz, 1H), 7.97−7.90 (m, 1H), 7.91−7.85 (m, 2H), 7.84−7.78 (m, 3H), 7.78−7.72 (m, 3H), 7.66−7.61 (m, 1H), 7.39−7.35 (m, 2H), 7.33−7.26 (m, 2H), 7.11 (ddd, J = 7.2, 5.9, 1.1 Hz, 1H), 7.05−6.97 (m, 4H), 6.91 (ddd, J = 8.2, 5.4, 4.9 Hz, 3H), 6.81−6.72 (m, 3H), 6.24 (d, J = 7.4 Hz, 1H), 6.07 (d, J = 7.4 Hz, 1H). ^{13}C NMR (101 MHz,) δ/ppm: 203.07, 167.67, 167.37, 156.87, 156.82, 156.39, 154.75, 153.56, 152.96, 152.92, 152.30, 152.24, 152.03, 151.07, 151.03, 150.11, 149.73, 149.39, 149.23, 148.85, 147.18, 146.52, 144.72, 144.38, 144.34, 143.72, 139.12, 139.07, 138.10, 137.62, 137.60, 136.24, 135.82, 135.55, 134.25, 134.24, 131.79, 131.78, 131.49, 130.75, 130.45, 129.66, 128.15, 127.84, 127.28, 127.27, 126.26, 126.25, 125.97, 125.59, 125.29, 124.47, 124.13, 124.02, 123.65, 123.62, 122.83, 122.58, 120.47, 120.36.

Stability Study of [1](ClO$_4$)$_2$. The stability of complex [**1**]$^{2+}$ was tested by dissolving it (0.1 mM) DMSO and diluted with 10 mM phosphate-buffered saline (PBS). The stability of [**1**]$^{2+}$ in PBS was studied by measuring its absorbance with time using a UV−vis spectrometer.

Preparation of a Stock Solution of [1](ClO$_4$)$_2$. Complex [**1**](ClO$_4$)$_2$ was dissolved in DMSO (Hybri-Max, sterile-filtered) to prepare 100 mM stock concentration. Then, the stock concentration of compounds was diluted (1000 times) directly in cell culture media to prepare a 100 μM working concentration. All other working concentrations were prepared by dilution of 100 μM working concentration. Stock solutions were stored at −20 °C, and working dilutions were always freshly prepared.

Cell Culture. Breast cancer cell line MCF-7 was grown in Dulbecco's modified Eagle's medium (DMEM) medium and MBA-MB-231 in RPMI as monolayer supplemented with 10% fetal bovine serum (FBS), 100 U/mL penicillin, and 100 μg/mL streptomycin at 37 °C in humid, 5% CO_2 atmosphere.

Growth Inhibition. The cytotoxic effect of [**1**](ClO$_4$)$_2$ was evaluated by the 3-(4,5-dimethylthiazol-2-yl)-2,5-diphenyltetrazolium bromide (MTT) assay. The cells (3×10^3 per well of 96-well plate) were seeded 24 h prior to the drug treatment. The cells were treated with different concentrations of the compounds (0−100 μM) for 48 h in triplicate. After 48 h of drug treatment, the MTT solution (20 μL of 5 mg/mL stock for each well) was added to the media and the cells were further allowed to be incubated for 3.5 h in a humid 5% CO_2 incubator. Then, the media containing the MTT solution was replaced by the MTT solvent (iso-propanol, 4 mM HCl, and 0.01% Triton X-100) and incubated for 15 min at room temperature, followed by gentle shaking to ensure the complete dissolution of Formazan. Finally, absorbance was measured at 590 nm using a Thermo Pierce Elisa plate reader. All experiments were carried out for at least three biological triplicates. The percentage of viable cells was calculated in comparison with the growth of vehicle-treated cells, and it was taken as 100%.

Cell Cycle Analysis. Exponentially growing MCF-7 cells were treated with 20 μM [**1**](ClO$_4$)$_2$ for 48 h. Similarly, the MDA-MB-231 cells were treated with 10 μM of [**1**](ClO$_4$)$_2$. The cells treated with 0.01% DMSO were considered as control. At the end of the treatment, the cells were washed with ice-cold PBS, fixed with 95% chilled ethanol, and kept at 4 °C for 24 h. Then, the fixed cells were washed again with ice-cold PBS to remove the trace amount of ethanol and stained with the staining solution comprising 50 μg/mL propidium iodide and 50 μg/mL RNAse in PBS. The cells were acquired on a BD FACS Calibur instrument, and the data was analyzed using Cell QuestPro software. All of the experiments were carried out in triplicate.

Western Blotting. Exponentially growing MCF-7 and MDA-MB-231 cells were treated with 20 and 10 μM of [**1**](ClO$_4$)$_2$, respectively, for 48 h. After 48 h of treatment, the cells were harvested and lysed with whole cell lysis buffer (50 mM Tris pH 7.4, 200 mM NaCl, 50 mM NaF, 1 mM Na_3VO_4, 0.5% Triton X-100, and protease inhibitor cocktail) in ice for 30 min.[85] Lysates were cleared by centrifuging at high speed (16,000g) for 20 min and the supernatants were transferred to new tubes. Protein concentration was measured by the Bradford method.[90] The samples were prepared and run in sodium dodecyl sulfate-polyacrylamide gel electrophoresis (SDS-PAGE) with Tris-glycine (25 mM Tris, 192 mM glycine) running buffer containing 0.1% SDS. The separated proteins were transferred onto the PVDF membrane with a transfer buffer (Tris-glycine containing 20% methanol). The antibodies specific for BAX, PUMA, cleaved caspase 3, LC3B, pAKT (S473), pERK, pMEK, MEK, and AKT were obtained from the cell signaling technology. Antibodies for p53, APAF, pJNK, JNK, and ERK were purchased from Santacruz Biotechnology. Tubulin and β-actin were purchased from Sigma-Aldrich. p62 was purchased from Abcam. HRP-conjugated secondary antibodies were purchased from GE Health Care, and the signals were detected using a supersignal chemiluminescence substrate (Pierce, Thermo Scientific).

Theoretical Calculation. All DFT calculations were performed using Gaussian 09 suite of quantum chemical programs.[94] The ground-state geometry of complex [**1**]$^{2+}$ was optimized in the gas phase with a hybrid exchange-correlation functional B3LYP.[95−98] The LANL2DZ basis set with an effective core potential was employed for Ir and Ru atoms,[99−102] while the 6-31G(D) basis set was used for other atoms.[103,104] Gaussian's pruned grid ultrafine was used for numerical calculation. SCF convergence criteria of 10^{-8} au were employed throughout the calculation. Vertical electronic singlet state excitation of optimized geometry of complex [**1**]$^{2+}$ was computed using the TDDFT formalism in the gas phase.[105−107] Gauss-Sum 3.0 software was used to evaluate the percentage contribution of different groups to each molecular orbital.[108]

Crystallography. The X-ray-quality crystals of [**1**](ClO$_4$)$_2$ were obtained by the slow evaporation of $(CH_3)_2SO$ solution at room temperature. The crystallographic studies were performed using a Bruker D8 venture instrument using Mo Kα radiation (λ_α = 0.71073 Å) at 273 (2) K. APEX 10 software was used for the data collection by using standard phi-omega scan techniques. The data were scaled and reduced using SAINT and XPREP software. The structures were solved by direct methods using XSHELL software, and full-matrix least-squares with XSHELL software was used for refinement by refining on F^2.[109] The positions of all of the atoms were obtained by direct methods. All nonhydrogen atoms were refined anisotropically. The remaining hydrogen atoms were placed in geometrically constrained positions and refined with isotropic temperature factors, generally 1.2Ueq of their parent atoms.

The CCDC number for [**1**](ClO$_4$)$_2$ is 2237997.

■ ASSOCIATED CONTENT

Supporting Information

The Supporting Information is available free of charge at https://pubs.acs.org/doi/10.1021/acs.inorgchem.3c00272.

^{1}H and ^{13}C NMR spectra, computational data, frontier orbitals energy tables, and FACS data (PDF)

https://doi.org/10.1021/acs.inorgchem.3c00272
Inorg. Chem. 2023, 62, 7003−7013

Accession Codes

CCDC 2237997 contains the supplementary crystallographic data for this paper. These data can be obtained free of charge via www.ccdc.cam.ac.uk/data_request/cif, or by emailing data_request@ccdc.cam.ac.uk, or by contacting The Cambridge Crystallographic Data Centre, 12 Union Road, Cambridge CB2 1EZ, UK; fax: +44 1223 336033.

AUTHOR INFORMATION

Corresponding Authors

Manas Kumar Santra − *National Centre for Cell Science, NCCS Complex, Pune University Campus Ganeshkhind, Pune 411007 Maharashtra, India*; Email: manas@nccs.res.in

Srikanta Patra − *School of Basic Sciences, Indian Institute of Technology Bhubaneswar, Jatni 752050 Odisha, India*; orcid.org/0000-0002-0611-4047; Email: srikanta@iitbbs.ac.in

Authors

Saumyaranjan Mishra − *School of Basic Sciences, Indian Institute of Technology Bhubaneswar, Jatni 752050 Odisha, India*

Suman Kumar Tripathy − *School of Basic Sciences, Indian Institute of Technology Bhubaneswar, Jatni 752050 Odisha, India*

Debasish Paul − *National Centre for Cell Science, NCCS Complex, Pune University Campus Ganeshkhind, Pune 411007 Maharashtra, India*

Paltan Laha − *School of Basic Sciences, Indian Institute of Technology Bhubaneswar, Jatni 752050 Odisha, India*

Complete contact information is available at: https://pubs.acs.org/10.1021/acs.inorgchem.3c00272

Notes

The authors declare no competing financial interest.

ACKNOWLEDGMENTS

The authors are thankful to the SERB, DST (CRG/2018/000173), New Delhi, India, for financial support.

REFERENCES

(1) Bouwman, E.; Reedijk, J. Structural and Functional Models Related to the Nickel Hydrogenases. *Coord. Chem. Rev.* **2005**, *249*, 1555−1581.

(2) Van der Vlugt, J. I. Cooperative Catalysis with First-Row Late Transition Metals. *Eur. J. Inorg. Chem.* **2012**, *2012*, 363−375.

(3) Allen, A. E.; MacMillan, D. W. C. Synergistic Catalysis: A Powerful Synthetic Strategy for New Reaction Development. *Chem. Sci.* **2012**, *3*, 633−658.

(4) Do, L. H.; Lippard, S. J. Toward Functional Carboxylate-Bridged Diiron Protein Mimics: Achieving Structural Stability and Conformational Flexibility Using a Macrocyclic Ligand Framework. *J. Am. Chem. Soc.* **2011**, *133*, 10568−10581.

(5) Wu, S.-H.; Burkhardt, S. E.; Yao, J.; Zhong, Y.-W.; Abruña, H. D. Near-Infrared Absorbing and Emitting RuII-PtII Heterodimetallic Complexes of Dpdpz (Dpdpz= 2, 3-Di (2-Pyridyl)-5, 6-Diphenylpyrazine. *Inorg. Chem.* **2011**, *50*, 3959−3969.

(6) Jiang, F. L.; Wong, W. K.; Zhu, X. J.; Zhou, G. J.; Wong, W. Y.; Wu, P. L.; Tam, H. L.; Cheah, K. W.; Ye, C.; Liu, Y. Synthesis, Characterization, and Photophysical Properties of Some Heterodimetallic Bisporphyrins of Ytterbium and Transition Metals-Enhancement and Lifetime Extension of Yb3+ Emission by Transition-Metal Porphyrin Sensitization. *Eur. J. Inorg. Chem.* **2007**, *2007*, 3365−3374.

(7) Edder, C.; Piguet, C.; Bünzli, J. C.; Hopfgartner, G. High-Spin Iron(II) as a Semitransparent Partner for Tuning Europium(III) Luminescence in Heterodimetallic d-f Complexes. *Chem. - Eur. J.* **2001**, *7*, 3014−3024.

(8) Wu, S.-H.; Shao, J.-Y.; Kang, H.-W.; Yao, J.; Zhong, Y.-W. Substituent and Solvent Effects on the Electrochemical Properties and Intervalence Transfer in Asymmetric Mixed-Valent Complexes Consisting of Cyclometalated Ruthenium and Ferrocene. *Chem. - Asian J.* **2013**, *8*, 2843−2850.

(9) Sabater, S.; Mata, J. A.; Peris, E. Hydrodefluorination of Carbon−Fluorine Bonds by the Synergistic Action of a Ruthenium−Palladium Catalyst. *Nat. Commun.* **2013**, *4*, No. 2553.

(10) Swindell, E. P.; Hankins, P. L.; Chen, H.; Miodragović, Đ. U.; O'Halloran, T. V. Anticancer Activity of Small Molecule and Nanoparticulate Arsenic(III) Complexes. *Inorg. Chem.* **2013**, *52*, 12292−12304.

(11) Ackerman, L. K. G.; Lovell, M. M.; Weix, D. J. Multimetallic Catalysed Cross-Coupling of Aryl Bromides with Aryl Triflates. *Nature* **2015**, *524*, 454−457.

(12) Zanardi, A.; Mata, J. A.; Peris, E. Well-Defined Ir/Pd Complexes with a Triazolyl-Diylidene Bridge as Catalysts for Multiple Tandem Reactions. *J. Am. Chem. Soc.* **2009**, *131*, 14531−14537.

(13) Shibasaki, M.; Yamamoto, Y. *Multimetallic Catalysts in Organic Synthesis*; John Wiley & Sons, Wiley-VCH, 2004.

(14) Buchwalter, P.; Rosé, J.; Braunstein, P.; Rosé, J.; Braunstein, P. Multimetallic Catalysis Based on Heterometallic Complexes and Clusters. *Chem. Rev.* **2015**, *115*, 28−126.

(15) Dehury, N.; Mishra, S. R.; Laha, P.; Patra, S. Tandem α/β-Alkylation and Transfer Hydrogenation by Heterodimetallic Ruthenium-Iridium Complex. *Inorg. Chim. Acta* **2020**, *511*, 119796−119802.

(16) Patra, S.; Maity, N. Recent Advances in (Hetero)Dimetallic Systems towards Tandem Catalysis. *Coord. Chem. Rev.* **2021**, *434*, No. 213803.

(17) Babak, M. V.; Ang, W. H. Multinuclear Organometallic Ruthenium-Arene Complexes for Cancer Therapy. In *Metallo-Drugs: Development and Action of Anticancer Agents*; Walter de Gruyter GmbH, 2018; pp 171−198.

(18) Kim, I.; Song, Y. H.; Singh, N.; Jeong, Y. J.; Kwon, J. E.; Kim, H.; Cho, Y. M.; Kang, S. C.; Chi, K. W. Anticancer Activities of Self-Assembled Molecular Bowls Containing a Phenanthrene-Based Donor and Ru(II) Acceptors. *Int. J. Nanomed.* **2015**, *10*, 143−153.

(19) Cook, T. R.; Stang, P. J. Recent Developments in the Preparation and Chemistry of Metallacycles and Metallacages via Coordination. *Chem. Rev.* **2015**, *115*, 7001−7045.

(20) Cook, T. R.; Vajpayee, V.; Lee, M. H.; Stang, P. J.; Chi, K. W. Biomedical and Biochemical Applications of Self-Assembled Metallacycles and Metallacages. *Acc. Chem. Res.* **2013**, *46*, 2464−2474.

(21) Mishra, A.; Jeong, Y. J.; Jo, J. H.; Kang, S. C.; Lah, M. S.; Chi, K. W. Anticancer Potency Studies of Coordination Driven Self-Assembled Arene−Ru-Based Metalla-Bowls. *ChemBioChem* **2014**, *15*, 695−700.

(22) Pelletier, F.; Comte, V.; Massard, A.; Wenzel, M.; Toulot, S.; Richard, P.; Picquet, M.; Le Gendre, P.; Zava, O.; Edafe, F.; Casini, A.; Dyson, P. J. Development of Bimetallic Titanocene-Ruthenium-Arene Complexes as Anticancer Agents: Relationships between Structural and Biological Properties. *J. Med. Chem.* **2010**, *53*, 6923−6933.

(23) Tripathy, S. K.; De, U.; Dehury, N.; Pal, S.; Kim, H. S.; Patra, S. Dinuclear [{(p-Cym)RuCl} 2 (μ-Phpy)](PF 6) 2 and Heterodinuclear [(Ppy) 2 Ir(μ-Phpy)Ru(p-Cym)Cl](PF 6) 2 Complexes: Synthesis, Structure and Anticancer Activity. *Dalton Trans.* **2014**, *43*, 14546−14549.

(24) Nagy, I.; Farkas, E.; Kasparkova, J.; Kostrhunova, H.; Brabec, V.; Buglyó, P. Synthesis and Characterization of (Ru(II), Co(III)) Heterobimetallic Complexes Formed with a 1,10-Phenanthroline Based Hydroxamic Acid Conjugate. *J. Organomet. Chem.* **2020**, *916*, No. 121265.

(25) Holbrook, R. J.; Weinberg, D. J.; Peterson, M. D.; Weiss, E. A.; Meade, T. J. Light-Activated Protein Inhibition through Photo-induced Electron Transfer of a Ruthenium(II)-Cobalt(III) Bimetallic Complex. *J. Am. Chem. Soc.* **2015**, *137*, 3379−3385.
(26) Serrano-Ruiz, M.; Aguilera-Sáez, L. M.; Lorenzo-Luis, P.; Padrón, J. M.; Romerosa, A. Synthesis and Antiproliferative Activity of the Heterobimetallic Complexes [RuClCp(PPh 3)-μ-DmoPTA-1κ P :2κ 2 N, N ′-MCl 2] (M = Co, Ni, Zn; DmoPTA = 3,7-Dimethyl-1,3,7-Triaza-5-Phosphabicyclo[3.3.1]Nonane). *Dalton Trans.* **2013**, *42*, 11212−11219.
(27) Tauchman, J.; Süss-Fink, G.; Štěpnička, P.; Zava, O.; Dyson, P. J. Arene Ruthenium Complexes with Phosphinoferrocene Amino Acid Conjugates: Synthesis, Characterization and Cytotoxicity. *J. Organomet. Chem.* **2013**, *723*, 233−238.
(28) Boselli, L.; Carraz, M.; Mazères, S.; Paloque, L.; González, G.; Benoit-Vical, F.; Valentin, A.; Hemmert, C.; Gornitzka, H. Synthesis, Structures, and Biological Studies of Heterobimetallic Au(I)-Ru(Ii) Complexes Involving N-Heterocyclic Carbene-Based Multidentate Ligands. *Organometallics* **2015**, *34*, 1046−1055.
(29) Fernández-Gallardo, J.; Elie, B. T.; Sanaú, M.; Contel, M. Versatile Synthesis of Cationic N-Heterocyclic Carbene−Gold(i) Complexes Containing a Second Ancillary Ligand. Design of Heterobimetallic Ruthenium−Gold Anticancer Agents. *Chem. Commun.* **2016**, *52*, 3155−3158.
(30) Batchelor, L. K.; Ortiz, D.; Dyson, P. J. Histidine Targeting Heterobimetallic Ruthenium(II)-Gold(I) Complexes. *Inorg. Chem.* **2019**, *58*, 2501−2513.
(31) Wenzel, M.; De Almeida, A.; Bigaeva, E.; Kavanagh, P.; Picquet, M.; Le Gendre, P.; Bodio, E.; Casini, A. New Luminescent Polynuclear Metal Complexes with Anticancer Properties: Toward Structure-Activity Relationships. *Inorg. Chem.* **2016**, *55*, 2544−2557.
(32) Bertrand, B.; Citta, A.; Franken, I. L.; Picquet, M.; Folda, A.; Scalcon, V.; Rigobello, M. P.; Le Gendre, P.; Casini, A.; Bodio, E. Gold(I) NHC-Based Homo- and Heterobimetallic Complexes: Synthesis, Characterization and Evaluation as Potential Anticancer Agents. *J. Biol. Inorg. Chem.* **2015**, *20*, 1005−1020.
(33) Khan, R. A.; Asim, A.; Kakkar, R.; Gupta, D.; Bagchi, V.; Arjmand, F.; Tabassum, S. A Chloro-Bridged Heterobimetallic (H6-Arene)Ruthenium-Organotin Complex as an Efficient Topoisomerase Iα Inhibitor. *Organometallics* **2013**, *32*, 2546−2551.
(34) Anderson, C. M.; Taylor, I. R.; Tibbetts, M. F.; Philpott, J.; Hu, Y.; Tanski, J. M. Hetero-Multinuclear Ruthenium(III)/Platinum(II) Complexes That Potentially Exhibit Both Antimetastatic and Antineoplastic Properties. *Inorg. Chem.* **2012**, *51*, 12917−12924.
(35) Ma, L.; Ma, R.; Wang, Z.; Yiu, S. M.; Zhu, G. Heterodinuclear Pt(Iv)−Ru(Ii) Anticancer Prodrugs to Combat Both Drug Resistance and Tumor Metastasis. *Chem. Commun.* **2016**, *52*, 10735−10738.
(36) Zhu, J.; Rodríguez-Corrales, J. A.; Prussin, R.; Zhao, Z.; Dominijanni, A.; Hopkins, S. L.; Winkel, B. S. J.; Robertson, J. L.; Brewer, K. J. Exploring the Activity of a Polyazine Bridged Ru(Ii)−Pt(Ii) Supramolecule in F98 Rat Malignant Glioma Cells. *Chem. Commun.* **2017**, *53*, 145−148.
(37) Ramu, V.; Gill, M. R.; Jarman, P. J.; Turton, D.; Thomas, J. A.; Das, A.; Smythe, C. A Cytostatic Ruthenium(II)-Platinum(II) Bis(Terpyridyl) Anticancer Complex That Blocks Entry into S Phase by up-Regulating P27KIP1. *Chem. - Eur. J.* **2015**, *21*, 9185−9197.
(38) Adriaenssens, L.; Liu, Q.; Chaux-Picquet, F.; Tasan, S.; Picquet, M.; Denat, F.; Le Gendre, P.; Marques, F.; Fernandes, C.; Mendes, F.; Gano, L.; Campello, M. P. C.; Bodio, E. Novel Heterobimetallic Radiotheranostic: Preparation, Activity, and Biodistribution. *ChemMedChem* **2014**, *9*, 1567−1573.
(39) Fernández-Gallardo, J.; Elie, B. T.; Sulzmaier, F. J.; Sanaú, M.; Ramos, J. W.; Contel, M. Organometallic Titanocene-Gold Compounds as Potential Chemotherapeutics in Renal Cancer. Study of Their Protein Kinase Inhibitory Properties. *Organometallics* **2014**, *33*, 6669−6681.
(40) Wenzel, M.; Bertrand, B.; Eymin, M. J.; Comte, V.; Harvey, J. A.; Richard, P.; Groessl, M.; Zava, O.; Amrouche, H.; Harvey, P. D.; Le Gendre, P.; Picquet, M.; Casini, A. Multinuclear Cytotoxic Metallodrugs: Physicochemical Characterization and Biological Properties of Novel Heteronuclear Gold-Titanium Complexes. *Inorg. Chem.* **2011**, *50*, 9472−9480.
(41) González-Pantoja, J. F.; Stern, M.; Jarzecki, A. A.; Royo, E.; Robles-Escajeda, E.; Varela-Ramírez, A.; Aguilera, R. J.; Contel, M. Titanocene-Phosphine Derivatives as Precursors to Cytotoxic Heterometallic TiAu 2 and TiM (M = Pd, Pt) Compounds. Studies of Their Interactions with DNA. *Inorg. Chem.* **2011**, *50*, 11099−11110.
(42) Lease, N.; Vasilevski, V.; Carreira, M.; De Almeida, A.; Sanaú, M.; Hirva, P.; Casini, A.; Contel, M. Potential Anticancer Heterometallic Fe-Au and Fe-Pd Agents: Initial Mechanistic Insights. *J. Med. Chem.* **2013**, *56*, 5806−5818.
(43) Riera, X.; Caubet, A.; López, C.; Moreno, V. Study of the Electrochemical Properties of Pd(II) and Pt(II) Complexes Containing Ferrocenyl Ligands and Their Interaction with DNA. *Polyhedron* **1999**, *18*, 2549−2555.
(44) Gimeno, M. C.; Goitia, H.; Laguna, A.; Luque, M. E.; Villacampa, M. D.; Sepúlveda, C.; Meireles, M. Conjugates of Ferrocene with Biological Compounds. Coordination to Gold Complexes and Antitumoral Properties. *J. Inorg. Biochem.* **2011**, *105*, 1373−1382.
(45) García-Moreno, E.; Gascon, S.; Rodriguez-Yoldi, M. J. M.; Cerrada, E.; Laguna, M.; García-Moreno, E.; Gascón, S.; Rodriguez-Yoldi, M. J. M.; Gascón, S.; Rodriguez-Yoldi, M. J. M.; Cerrada, E.; Laguna, M. S-Propargylthiopyridine Phosphane Derivatives As Anticancer Agents: Characterization and Antitumor Activity. *Organometallics* **2013**, *32*, 3710−3720.
(46) Vanicek, S.; Kopacka, H.; Wurst, K.; Vergeiner, S.; Kankowski, S.; Schur, J.; Bildstein, B.; Ott, I. Cobaltoceniumethynyl Gold(i) as an Unusual Heterodinuclear Bioorganometallic Fragment to Study the Biological Properties of Alkynyl Gold Complexes. *Dalton Trans.* **2016**, *45*, 1345−1348.
(47) Luengo, A.; Fernández-Moreira, V.; Marzo, I.; Gimeno, M. C. Bioactive Heterobimetallic Re(I)/Au(I) Complexes Containing Bidentate N-Heterocyclic Carbenes. *Organometallics* **2018**, *37*, 3993−4001.
(48) Fernández-Moreira, V.; Marzo, I.; Gimeno, M. C. Luminescent Re(I) and Re(I)/Au(I) Complexes as Cooperative Partners in Cell Imaging and Cancer Therapy. *Chem. Sci.* **2014**, *5*, 4434−4446.
(49) Bertrand, B.; Botuha, C.; Forté, J.; Dossmann, H.; Salmain, M. A Bis-Chelating/Ligand for the Synthesis of Heterobimetallic Platinum(II)/Rhenium(I) Complexes: Tools for the Optimization of a New Class of Platinum(II) Anticancer Agents. *Chem. - Eur. J.* **2020**, *26*, 12846−12861.
(50) Redrado, M.; Benedi, A.; Marzo, I.; García-Otín, A. L.; Fernández-Moreira, V.; Concepción Gimeno, M. Multifunctional Heterometallic IrIII−AuI Probes as Promising Anticancer and Antiangiogenic Agents. *Chem. - Eur. J.* **2021**, *27*, 9885−9897.
(51) Wang, J.; Sun, S.; Mu, D.; Wang, J.; Sun, W.; Xiong, X.; Qiao, B.; Peng, X. A Heterodinuclear Complex OsIr Exhibiting Near-Infrared Dual Luminescence Lights Up the Nucleoli of Living Cells. *Organometallics* **2014**, *33*, 2681−2684.
(52) Li, H.; Lan, R.; Chan, C. F.; Jiang, L.; Dai, L.; Kwong, D. W. J.; Lam, M. H. W.; Wong, K. L. Real-Time in Situ Monitoring via Europium Emission of the Photo-Release of Antitumor Cisplatin from a Eu−Pt Complex. *Chem. Commun.* **2015**, *51*, 14022−14025.
(53) Fernández-Gallardo, J.; Elie, B. T.; Sadhukha, T.; Prabha, S.; Sanaú, M.; Rotenberg, S. A.; Ramos, J. W.; Contel, M. Heterometallic Titanium−Gold Complexes Inhibit Renal Cancer Cells in Vitro and in Vivo. *Chem. Sci.* **2015**, *6*, 5269−5283.
(54) Bjelosevic, H.; Guzei, I. A.; Spencer, L. C.; Persson, T.; Kriel, F. H.; Hewer, R.; Nell, M. J.; Gut, J.; Van Rensburg, C. E. J.; Rosenthal, P. J.; Coates, J.; Darkwa, J.; Elmroth, S. K. C. Platinum(II) and Gold(I) Complexes Based on 1,1′-Bis(Diphenylphosphino)-Metallocene Derivatives: Synthesis, Characterization and Biological Activity of the Gold Complexes. *J. Organomet. Chem.* **2012**, *720*, 52−59.

https://doi.org/10.1021/acs.inorgchem.3c00272
Inorg. Chem. 2023, 62, 7003−7013

(55) Siewert, B.; van Rixel, V. H. S.; van Rooden, E. J.; Hopkins, S. L.; Moester, M. J. B.; Ariese, F.; Siegler, M. A.; Bonnet, S. Chemical Swarming: Depending on Concentration, an Amphiphilic Ruthenium Polypyridyl Complex Induces Cell Death via Two Different Mechanisms. *Chem. - Eur. J.* **2016**, *22*, 10960−10968.
(56) Wragg, A.; Gill, M. R.; Turton, D.; Adams, H.; Roseveare, T. M.; Smythe, C.; Su, X.; Thomas, J. A. Tuning the Cellular Uptake Properties of Luminescent Heterobimetallic Iridium(III)−Ruthenium(II) DNA Imaging Probes. *Chem. - Eur. J.* **2014**, *20*, 14004−14011.
(57) Laha, P.; Chandra, F.; Husain, A.; Koner, A. L.; Patra, S. Long-Lived Cyclometallated Iridium Complexes: Synthesis, Structure, DFT and Photocatalytic Aspects. *Dyes Pigm.* **2022**, *197*, No. 109925.
(58) Chandra, F.; Pal, K.; Koner, A. L. Tailoring Emission Properties Using Macrocyclic Nanocavities via Guest Interplay in Aqueous Solution. *ChemistrySelect* **2016**, *1*, 6156−6159.
(59) Lu, X.-H.; Shi, S.; Yao, J.-L.; Gao, X.; Huang, H.-L.; Yao, T.-M. Two Structurally Analogous Ruthenium Complexes as Naked-Eye and Reversible Molecular "Light Switch" for G-Quadruplex DNA. *J. Inorg. Biochem.* **2014**, *140*, 64−71.
(60) Chen, J. P.; Li, X.-C. Organic Light-Emitting Device Having Phenanthroline-Fused Phenazine. U.S. Patent US6713781B12004.
(61) Sessler, B.; Andrioletti, A. C.; Try, C. B.; Sessler, J.; Andrioletti, B.; Try Andrew Carl, B. C.; Sessler, B.; Andrioletti, A. C.; Try, C. B. Colormetric Sensor Compositions and Methods. U.S. Patent US6482949B12000.
(62) Tripathy, S. K.; De, U.; Dehury, N.; Laha, P.; Panda, M. K.; Kim, H. S.; Patra, S. Cyclometallated Iridium Complexes Inducing Paraptotic Cell Death like Natural Products: Synthesis, Structure and Mechanistic Aspects. *Dalton Trans.* **2016**, *45*, 15122−15136.
(63) Ghumaan, S.; Sarkar, B.; Patra, S.; Parimal, K.; Van Slageren, J.; Fiedler, J.; Kaim, W.; Lahiri, G. K. 3,6-Bis(2′-Pyridyl)Pyridazine (L) and Its Deprotonated Form (L − H+)- as Ligands for {(Acac)2Run+} or {(Bpy)2Rum+}: Investigation of Mixed Valency in [{(Acac)-2Ru}2(μ-L − H+)]0 and [{(Bpy)2Ru}2(μ-L − H+)]4+ by Spectroelectrochemistry and EPR. *Dalton Trans.* **2005**, 706−712.
(64) Shao, J. Y.; Fu, N.; Yang, W. W.; Zhang, C. Y.; Zhong, Y. W.; Lin, Y.; Yao, J. Cyclometalated Ruthenium(Ii) Complexes with Bis(Benzimidazolyl)Benzene for Dye-Sensitized Solar Cells. *RSC Adv.* **2015**, *5*, 90001−90009.
(65) Otsuki, J.; Takamori, Y.; Sugawa, K.; Islam, A.; Ogawa, K.; Yamano, A.; Yoshikawa, I.; Araki, K. Heteroleptic Ruthenium Complexes with 6-(Ortho-Substituted Phenyl)-2,2′-Bipyridine Derivatives. *J. Organomet. Chem.* **2014**, *749*, 312−319.
(66) Sui, L.-Z.; Yang, W.-W.; Yao, C.-J.; Xie, H.-Y.; Zhong, Y.-W. Charge Delocalization of 1,4-Benzenedicyclometalated Ruthenium: A Comparison between Tris-Bidentate and Bis-Tridentate Complexes. *Inorg. Chem.* **2012**, *51*, 1590−1598.
(67) Constable, E. C.; Rees, D. G. F. Convergent Metal-Directed and Divergent Approaches to Multiply Cyclometalated Complexes. *Polyhedron* **1998**, *17*, 3281−3289.
(68) Constable, E. C.; Thompson, A. M. W. C. Metallosupramolecular Oligomers—Diruthenium Complexes of a Novel Ligand Incorporating N,N′,N″ and N,N′,C Metal-Binding Domains. *Supramol. Chem.* **1994**, *4*, 95−99.
(69) Constable, E. C.; Thompson, A. M. W. C. Metallosupramolecular Assemblies Incorporating Cyclometallating Analogs of 2,2′:6′,2″-Terpyridine Domains. *New J. Chem.* **1996**, *20*, 65−82.
(70) Patoux, C.; Launay, J.-P.; Beley, M.; Chodorowski-Kimmes, S.; Collin, J.-P.; James, S.; Sauvage, J.-P. Long-Range Electronic Coupling in Bis(Cyclometalated) Ruthenium Complexes. *J. Am. Chem. Soc.* **1998**, *120*, 3717−3725.
(71) Kreitner, C.; Erdmann, E.; Seidel, W. W.; Heinze, K. Understanding the Excited State Behavior of Cyclometalated Bis(Tridentate)Ruthenium(II) Complexes: A Combined Experimental and Theoretical Study. *Inorg. Chem.* **2015**, *54*, 11088−11104.
(72) Huang, H.; Zhang, P.; Chen, Y.; Qiu, K.; Jin, C.; Ji, L.; Chao, H. Synthesis, Characterization and Biological Evaluation of Labile Intercalative Ruthenium(II) Complexes for Anticancer Drug Screening. *Dalton Trans.* **2016**, *45*, 13135−13145.
(73) Albani, B. A.; Peña, B.; Saha, S.; White, J. K.; Schaeffer, A. M.; Dunbar, K. R.; Turro, C. A Dinuclear Ru(Ii) Complex Capable of Photoinduced Ligand Exchange at Both Metal Centers. *Chem. Commun.* **2015**, *51*, 16522−16525.
(74) Patra, S.; Sarkar, B.; Ghumaan, S.; Patil, M. P.; Mobin, S. M.; Sunoj, R. B.; Kaim, W.; Lahiri, G. K. Isomeric Ruthenium Terpyridine Complexes [Ru (Trpy)(L) Cl] N+ Containing the Unsymmetrically Bidentate Acceptor L= 3-Amino-6-(3, 5-Dimethylpyrazol-1-Yl)-1, 2, 4, 5-Tetrazine. Synthesis, Structures, Electrochemistry, Spectroscopy and DFT Calculations. *Dalton Trans.* **2005**, 1188−1194.
(75) Lo, K. K.-W.; Li, S. P.-Y.; Zhang, K. Y. Development of Luminescent Iridium(Iii) Polypyridine Complexes as Chemical and Biological Probes. *New J. Chem.* **2011**, *35*, 265−287.
(76) Lo, K.-W.; Chung, C.; Zhu, N. Nucleic Acid Intercalators and Avidin Probes Derived from Luminescent Cyclometalated Iridium (III)−Dipyridoquinoxaline and-Dipyridophenazine Complexes. *Chem. - Eur. J.* **2006**, *12*, 1500−1512.
(77) Li, S.-Y.; Liu, H.; Zhang, K. Y.; Lo, K. K. Modification of Luminescent Iridium (III) Polypyridine Complexes with Discrete Poly (Ethylene Glycol)(PEG) Pendants: Synthesis, Emissive Behavior, Intracellular Uptake, and PEGylation Properties. *Chem. - Eur. J.* **2010**, *16*, 8329−8339.
(78) Lau, J. S.-Y.; Lee, P.-K.; Tsang, K. H.-K.; Ng, C. H.-C.; Lam, Y.-W.; Cheng, S.-H.; Lo, K. K.-W. Luminescent Cyclometalated Iridium (III) Polypyridine Indole Complexes- Synthesis, Photophysics, Electrochemistry, Protein-Binding Properties, Cytotoxicity, and Cellular Uptake. *Inorg. Chem.* **2009**, *48*, 708−718.
(79) Yang, W.-W.; Yao, J.; Zhong, Y.-W. Redox-Asymmetric Bisruthenium Complex Bridged by a Pyridin-4-Yl Moiety: Synthesis, Characterization, and Electronic Coupling Studies. *Organometallics* **2012**, *31*, 8577−8583.
(80) Jin, C.; Liu, J.; Chen, Y.; Li, G.; Guan, R.; Zhang, P.; Ji, L.; Chao, H. Cyclometalated Iridium (Iii) Complexes with Imidazo [4, 5-f][1, 10] Phenanthroline Derivatives for Mitochondrial Imaging in Living Cells. *Dalton Trans.* **2015**, *44*, 7538−7547.
(81) Kostova, I. Ruthenium Complexes as Anticancer Agents. *Curr. Med. Chem.* **2006**, *13*, 1085−1107.
(82) Süss-Fink, G. Arene Ruthenium Complexes as Anticancer Agents. *Dalton Trans.* **2010**, *39*, 1673−1688.
(83) Liu, Z.; Sadler, P. J. Organoiridium Complexes: Anticancer Agents and Catalysts. *Acc. Chem. Res.* **2014**, *47*, 1174−1185.
(84) Yang, T.; Zhu, M.; Jiang, M.; Yang, F.; Zhang, Z. Current Status of Iridium-Based Complexes against Lung Cancer. *Front. Pharmacol.* **2022**, No. 4029.
(85) Manne, R. K.; Agrawal, Y.; Malonia, S. K.; Banday, S.; Edachery, S.; Patel, A.; Kumar, A.; Shetty, P.; Santra, M. K. FBXL20 Promotes Breast Cancer Malignancy by Inhibiting Apoptosis through Degradation of PUMA and BAX. *J. Biol. Chem.* **2021**, *297*, No. 101253.
(86) Zhou, H.; Li, X. M.; Meinkoth, J.; Pittman, R. N. Akt Regulates Cell Survival and Apoptosis at a Postmitochondrial Level. *J. Cell Biol.* **2000**, *151*, 483−494.
(87) Wang, R. C.; Wei, Y.; An, Z.; Zou, Z.; Xiao, G.; Bhagat, G.; White, M.; Reichelt, J.; Levine, B. Akt-Mediated Regulation of Autophagy and Tumorigenesis through Beclin 1 Phosphorylation. *Science* **2012**, *338*, 956−959.
(88) Lee, C. S.; Lee, L. C.; Yuan, T. L.; Chakka, S.; Fellmann, C.; Lowe, S. W.; Caplen, N. J.; McCormick, F.; Luo, J. MAP Kinase and Autophagy Pathways Cooperate to Maintain RAS Mutant Cancer Cell Survival. *Proc. Natl. Sci. U.S.A.* **2019**, *116*, 4508−4517.
(89) Dhanasekaran, D. N.; Reddy, E. P. JNK Signaling in Apoptosis. *Oncogene* **2008**, *27*, 6245−6251.
(90) Chinni, S. R.; Sarkar, F. H. Akt Inactivation Is a Key Event in Indole-3-Carbinol-Induced Apoptosis in PC-3 Cells. *Clin. Cancer Res.* **2002**, *8*, 1228−1236.
(91) Bessel, C. A.; Leising, R. A.; Szczepura, L. F.; Perez, W. J.; Huyhn, M. H. V.; Takeuchi, K. J.; Brewer, K. J.; Jones, S. W.

https://doi.org/10.1021/acs.inorgchem.3c00272
Inorg. Chem. 2023, 62, 7003−7013

Trichloro[2,2′:6′,2″-Terpyridine]Ruthenium(III) and Phosphine Ligand Derivatives. *Inorg. Synth.* **1998**, 186−198.
(92) Nonoyama, M. Benzo[h]Quinolin-10-Yl-N Iridium(III) Complexes. *Bull. Chem. Soc. Jpn.* **1974**, *47*, 767−768.
(93) Bodige, S.; MacDonnell, F. M. Synthesis of Free and Ruthenium Coordinated 5,6-Diamino-1,10-Phenanthroline. *Tetrahedron Lett.* **1997**, *38*, 8159−8160.
(94) Frisch, M. J.; Trucks, G. W.; Schlegel, H. B.; Scuseria, G. E.; Robb, M. A.; Cheeseman, J. R.; Scalmani, G.; Barone, V.; Mennucci, B.; Petersson, G. A.; Nakatsuji, H.; Caricato, M.; Li, X.; Hratchian, H. P.; Izmaylov, A. F.; Bloino, J.; Zheng, G.; Sonnenberg, J. L.; Hada, M.; Ehara, M.; Toyota, K.; Fukuda, R.; Hasegawa, J.; Ishida, M.; Nakajima, T.; Honda, Y.; Kitao, O.; Nakai, H.; Vreven, T.; Montgomery, J. A., Jr.; Peralta, J. E.; Ogliaro, F.; Bearpark, M. J.; Heyd, J.; Brothers, E. N.; Kudin, K. N.; Staroverov, V. N.; Kobayashi, R.; Normand, J.; Raghavachari, K.; Rendell, A. P.; Burant, J. C.; Iyengar, S. S.; Tomasi, J.; Cossi, M.; Rega, N.; Millam, N. J.; Klene, M.; Knox, J. E.; Cross, J. B.; Bakken, V.; Adamo, C.; Jaramillo, J.; Gomperts, R.; Stratmann, R. E.; Yazyev, O.; Austin, A. J.; Cammi, R.; Pomelli, C.; Ochterski, J. W.; Martin, R. L.; Morokuma, K.; Zakrzewski, V. G.; Voth, G. A.; Salvador, P.; Dannenberg, J. J.; Dapprich, S.; Daniels, A. D.; Farkas, Ö.; Foresman, J. B.; Ortiz, J. V.; Cioslowski, J.; Fox, D. J. *Gaussian 09*; Gaussian, Inc.: Wallingford, CT, USA, 2009.
(95) Becke, A. D. Density-functional Thermochemistry. III. The Role of Exact Exchange. *J. Chem. Phys.* **1993**, *98*, 5648−5652.
(96) Vosko, S. H.; Wilk, L.; Nusair, M. Accurate Spin-Dependent Electron Liquid Correlation Energies for Local Spin Density Calculations: A Critical Analysis. *Can. J. Phys.* **1980**, *58*, 1200−1211.
(97) Lee, C.; Yang, W.; Parr, R. G. Development of the Colle-Salvetti Correlation-Energy Formula into a Functional of the Electron Density. *Phys. Rev. B* **1988**, *37*, 785−789.
(98) Stephens, P. J.; Devlin, F. J.; Chabalowski, Cf.; Frisch, M. J. Ab Initio Calculation of Vibrational Absorption and Circular Dichroism Spectra Using Density Functional Force Fields. *J. Phys. Chem. A* **1994**, *98*, 11623−11627.
(99) Hay, P. J.; Wadt, W. R. Ab Initio Effective Core Potentials for Molecular Calculations. Potentials for the Transition Metal Atoms Sc to Hg. *J. Chem. Phys.* **1985**, *82*, 270−283.
(100) Hay, P. J.; Wadt, W. R. Ab Initio Effective Core Potentials for Molecular Calculations. Potentials for K to Au Including the Outermost Core Orbitals. *J. Chem. Phys.* **1985**, *82*, 299−310.
(101) Wadt, W. R.; Hay, P. J. Ab Initio Effective Core Potentials for Molecular Calculations. Potentials for Main Group Elements Na to Bi. *J. Chem. Phys.* **1985**, *82*, 284−298.
(102) Dunning, T. H., Jr; Hay, P. J. Gaussian Basis Sets for Molecular Calculations. In *Modern Theoretical Chemistry*; Schaefer, H. F., III, Ed.; Springer: New York, 1976; Vol. 3.
(103) Francl, M. M.; Pietro, W. J.; Hehre, W. J.; Binkley, J. S.; Gordon, M. S.; DeFrees, D. J.; Pople, J. A. Self-consistent Molecular Orbital Methods. XXIII. A Polarization-type Basis Set for Second-row Elements. *J. Chem. Phys.* **1982**, *77*, 3654−3665.
(104) Hariharan, P. C.; Pople, J. A. The Influence of Polarization Functions on Molecular Orbital Hydrogenation Energies. *Theor. Chim. Acta* **1973**, *28*, 213−222.
(105) Bauernschmitt, R.; Ahlrichs, R. Treatment of Electronic Excitations within the Adiabatic Approximation of Time Dependent Density Functional Theory. *Chem. Phys. Lett.* **1996**, *256*, 454−464.
(106) Stratmann, R. E.; Scuseria, G. E.; Frisch, M. J. An Efficient Implementation of Time-Dependent Density-Functional Theory for the Calculation of Excitation Energies of Large Molecules. *J. Chem. Phys.* **1998**, *109*, 8218−8224.
(107) Casida, M. E.; Jamorski, C.; Casida, K. C.; Salahub, D. R. Molecular Excitation Energies to High-Lying Bound States from Time-Dependent Density-Functional Response Theory: Characterization and Correction of the Time-Dependent Local Density Approximation Ionization Threshold. *J. Chem. Phys.* **1998**, *108*, 4439−4449.
(108) O'boyle, N. M.; Tenderholt, A. L.; Langner, K. M. Cclib: A Library for Package-Independent Computational Chemistry Algorithms. *J. Comput. Chem.* **2008**, *29*, 839−845.
(109) Sheldrick, G. M. IUCr. A Short History of SHELX. *Acta Crystallogr., Sect. A: Found. Crystallogr.* **2008**, *64*, 112−122.

https://doi.org/10.1021/acs.inorgchem.3c00272
Inorg. Chem. 2023, 62, 7003−7013